URTeC: 2435484

A Geomechanical Study of Refracturing based on Microseismic Observations – Case Study of Haynesville and Eagle Ford Wells

Alireza Agharazi*, Sudhendu Kashikar, MicroSeismic Inc.

This paper was prepared for presentation at the Unconventional Resources Technology Conference held in San Antonio, Texas, USA, 1-3 August 2016.

Summary

Microseismic monitoring of refracturing of depleted horizontal wells frequently shows a concentration of microseismic activity at the heel area when no mechanical isolation is used. This observation suggests that a considerable length of the well toward the toe does not benefit from refracturing and remains unstimulated. Different completion techniques, ranging from injecting diverters to using mechanical intervention methods, are usually used to avoid the localized stimulation and to enhance the treatment effectiveness. However, often overlooked is the effect of the reservoir rock's mechanical characteristics and how they contribute to the treatment results.

In this study we investigated the potential contributing factors to the observed microseismic response: i) fluid pressure drop along the lateral, ii) diverter ineffectiveness, and iii) stimulation of pre-existing fractures versus developing fresh fractures from new perforations. Estimation of pressure losses along the well for the common casing diameters and fracturing fluids indicates that a high pressure gradient develops along the well during refracturing. It results in significantly higher injection pressures at the heel than at the toe, leading to higher discharge rates at the heel. If the added diverters fail to seal off the perforations at the heel area, this condition persists throughout the treatment and causes the localized stimulation of the rock, as is usually observed by microseismic monitoring.

The numerical simulation of refracturing indicates that under a non-uniform treatment pressure profile and in the absence of effective diverters, the initiation and propagation of new hydraulic fractures is unlikely. The dominant stimulation mechanism is the shear failure of natural fractures, driven by the increase of fluid pressure by injection of fluid through the old perforations. This result is consistent with the observed long delay in microseismic response to refracturing and the increasing event counts as pumping continues.

Based on these findings, we developed an alternative refracturing method that aims at increasing the reservoir effective complexity and enhancing the conductivity of the pre-existing hydraulic fractures uniformly along the well. The proposed method consists of a prolonged low-pressure and low-rate pad stage to pressurize the reservoir, followed by a high-pressure injection stage to stimulate the pressurized natural fractures and to place proppant in the new fractures. Critical to the success of this method is to avoid a high pressure contrast along the well. This can be achieved by proper selection of injection pressure and fluid viscosity with respect to the reservoir stresses and pressure, and the well characteristics. Numerical simulations indicate that the proposed method can considerably enhance the efficiency of refracturing, at no additional cost compared to the common refracturing methods.

1. **Introduction**

Refracturing of horizontal wells often provides a more economical alternative to drilling and completing of a new well for production uplift in a declining well. In a general sense, refracturing refers to the treatment of a previously stimulated well that has been under production for a while. The main objective of refracturing is to uplift production in a declining well, which can be achieved either by contacting new rock or by improving the conductivity of pre-existing fractures that have lost conductivity due to proppant embedment or poor initial stimulation (Vincent 2010, Nagel 2016).

Refracturing of horizontal wells often offers an economically appealing alternative to drilling and completing a new well for production enhancement, in that it eliminates drilling costs and associated operational costs. However, the final economic profitability of refracturing is a matter of balance between the treatment costs and the added production value. Two important factors that can potentially cause economic failure of refracturing are bad candidate selection and poor treatment.

Study of the refracturing design data in several recently treated horizontal wells shows that in most cases, the design parameters used for refracturing are very similar to the ones used for the initial stimulation of the same well or pad. This indicates that in most cases, the effect that initial stimulation and subsequent production have on the reservoir's mechanical parameters are ignored. From a geomechanical perspective, the most important changes in the reservoir condition that must be taken into account in the design of refracturing are:

- Altered reservoir stresses due to pressure depletion. This might be varied along the well.
- Existence of the previously stimulated propped or un-propped fractures, which provide pathways to the injected fluid, even without breaking new rock.
- Increased flow capacity of the formation due to previous stimulations.

The lower instantaneous shut-in pressures (ISIPs) and fracture closure pressures reported by several authors (Diakhate et al. 2015, Lanzet et al. 2007, Kashikar and Jbeili 2015) and the delayed microseismic response to pumping are two field observations indicating these changes in the reservoir condition. Diakhate et al. (2015) reported a 1,000–1,200 psi drop in ISIP for one refractured well and up to 3,000 psi reduction in the closure pressure for another refractured well.

In most refracturing treatments of horizontal wells, no mechanical stage isolation is used. The fluid is bullheaded, relying on diverting agents to move refracturing down the lateral. The main disadvantage of this method is lack of control on where the diverters sit along the lateral and which part of the well is benefiting from refracturing. When new perforations are added, reservoir pressure and stress heterogeneity along the well have a significant effect on whether fresh fractures are created from newly added perforations or pre-existing fractures (connected to the old perforations) are injected into. Bypassing of the intact reservoir (between the old perforations) is likely if the added diverters fail to function as intended. Non-uniform stimulation of the well, as is usually observed by concentration of microseismic events at the heel area, is another problem that usually occurs due to failure of diverters (Sudhendu and Jbeili 2015). These factors can greatly impact the economic viability of refracturing.

In this paper, we provide three case studies where microseismic monitoring shows the inefficiency of diverters and the localized stimulation toward the heel. We investigate the probable causes for the observed microseismic response by running numerical simulations of a generic refracturing model. The simulations show how the combined effect of pressure drop along the lateral and failure of diverters in plugging off the perforations leads to the observed microseismic response. We also studied the effect of stress and pressure changes on the reservoir response to refracturing treatments. By including all these factors, an alternative refracturing method is suggested that aims at adding effective complexity and improving the pre-existing fractures' conductivity. The efficiency of the proposed method was examined by numerical simulations.

2. Refracturing Case Studies – Microseismic Observations

The study of microseismic data from several re-fractured horizontal wells shows that the typical microseismic response in these wells includes:

- The concentration of microseismic events toward the heel.
- A time lag of several hours between the start of pumping and the onset of microseismic activity.

We studied three re-fractured wells in the Haynesville and Eagle Ford formations (well A, well B, and well C). The total pumping times (excluding break times) were recorded as 34 hours for well A, 42 hours for well B, and 49 hours for well C, with a pumping rate of 60–70 bbl/min. In all three wells, new perforations were added between the old ones (initial stage spacing 250–320 ft). Bio-balls were used to plug off the perforations and divert the slurry down the lateral after each pumping stage (no mechanical stage isolation was applied).

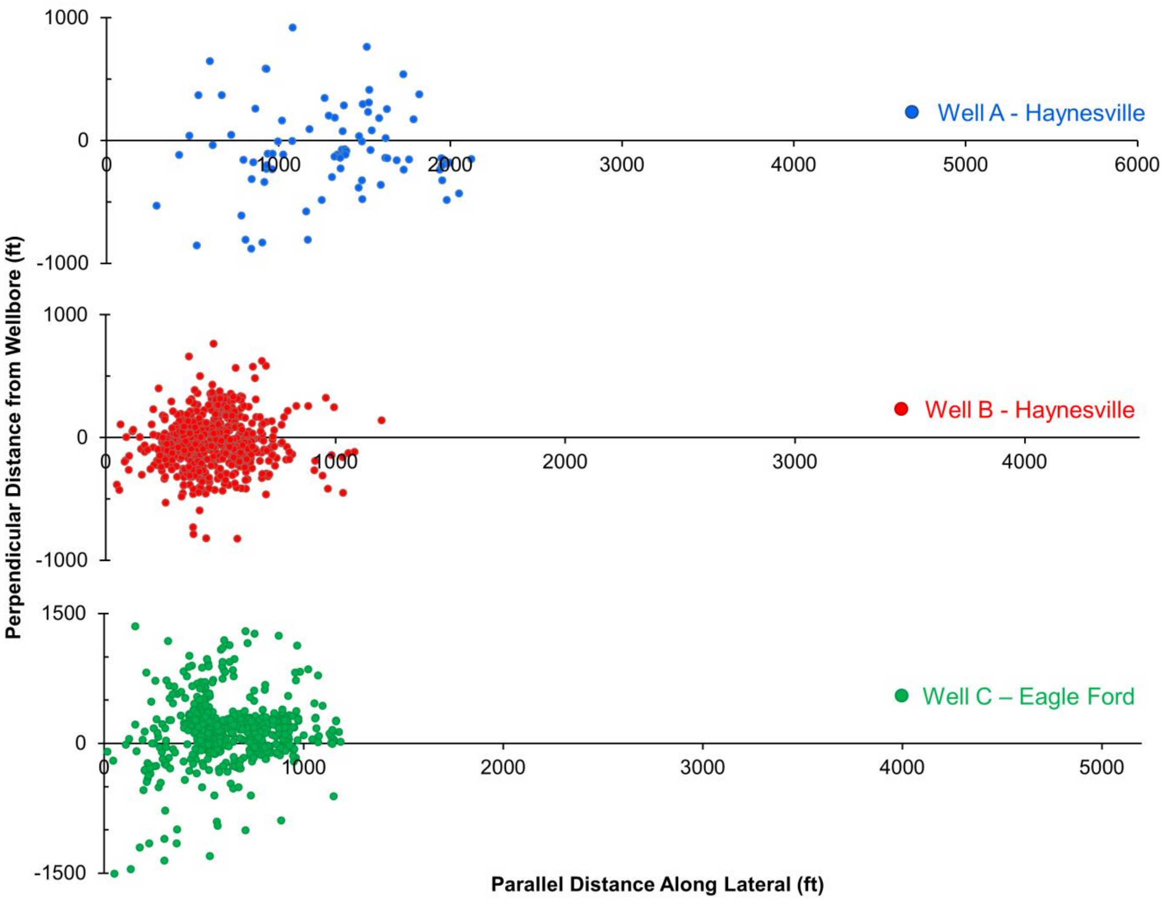

Figure 1: Distribution of microseismic events for the three horizontal wells in Haynesville and Eagle Ford. Pumping times were 36 hours for well A, 40 hours for well B, and 49 hours for well C (excluding pumping break times).

As shown in Figure 1, almost all microseismic events occurred at the first 20–30% of the lateral length in all three wells, suggesting that a considerable length of the wells were left unstimulated. It should be noted that in all three wells, the microseismic events were acquired using surface geophone arrays; therefore, no bias toward the observation well is expected, as might be the case when downhole microseismic tools are used.

Figure 2 shows the microseismic event counts versus cumulative injected slurry for the studied wells. In all cases, it took several hours of pumping (7–18 hours) before any microseismicity was recorded. The volume of slurry injected during this microseismically "silent" period ranged from 13,000 to 40,000 bbl.

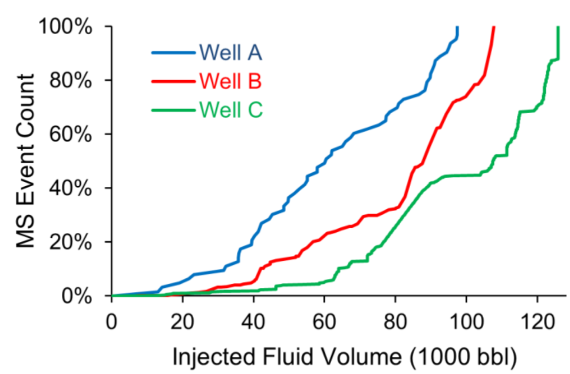

Figure 2: Microseismic event counts versus cumulative injected fluid volume. The volume of slurry injected during the silent period, when no microseismic events are detected, is 13,000 bbl for well A, 20,000 bbl for well B, and 40,000 for well C.

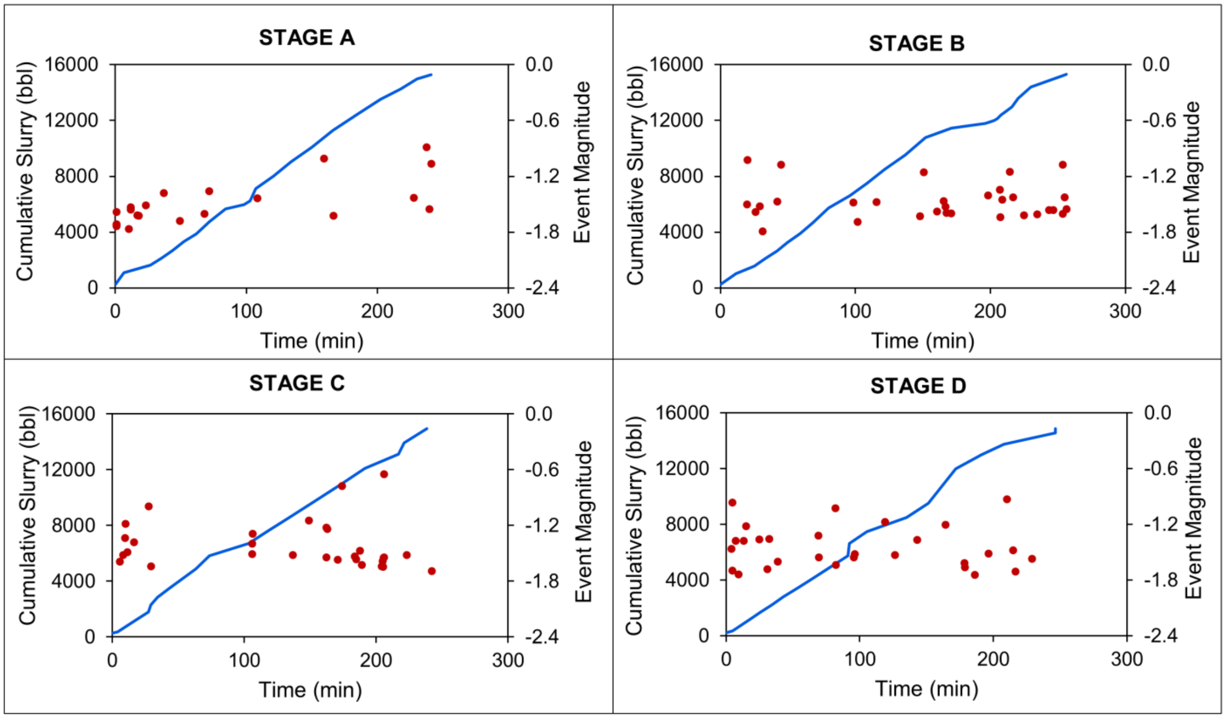

Figure 3: Cumulative slurry versus time graphs, with microseismic event time sequence and magnitude for four consecutive fracturing stages in well 1. Average pumping rate is 65 bbl/min.

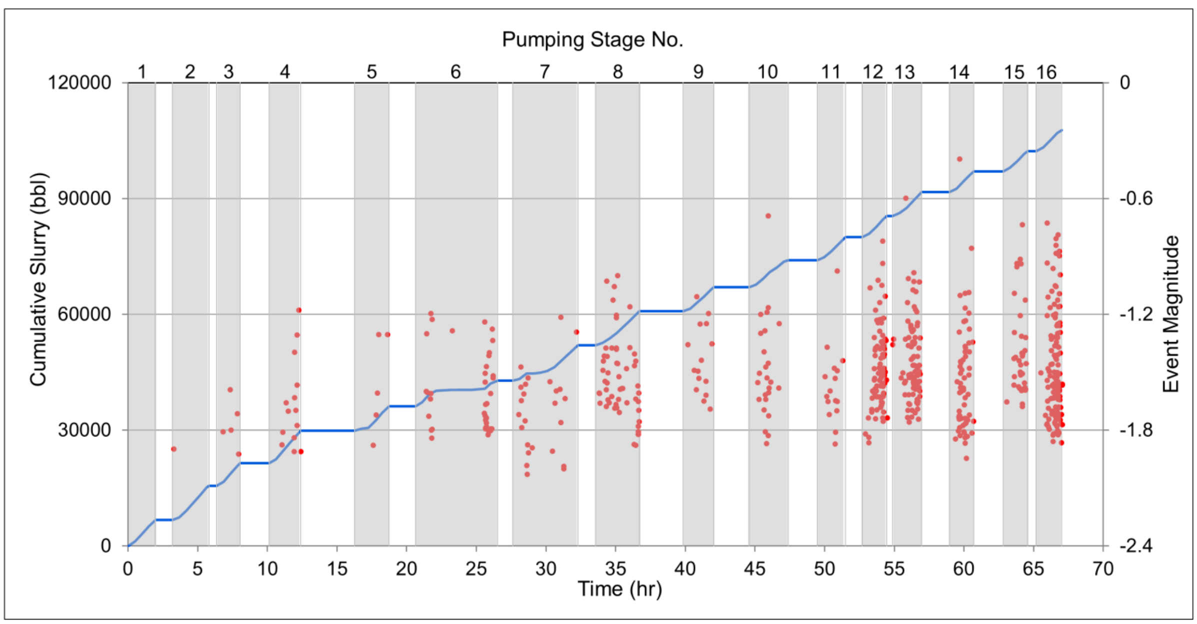

Figure 4: Cumulative slurry versus treatment time graphs, with microseismic event time sequence and magnitudes for 16 stages of refracturing in well 2. Major microseismic events start after 7 hours of treatment and injection of about 20,000 barrels of slurry. Average pumping rate is 65 bbl/min.

In order to show the difference between the common microseismic response to refracturing with that of fracturing we selected two wells in two adjacent pads (well 1 and well 2). Both wells were stimulated simultaneously and were monitored using the same surface microseismic arrays. Well 1 was a new well and was treated by hydraulic fracturing using slickwater and the plug-and-perf method. Well 2 was a depleted well and was re-stimulated using slickwater and bio-balls. In both case an injection rate of 65 bbl/min was applied. Figure 3 shows the cumulative slurry and microseismic events versus time for four consecutive stages of the fracturing well (well 1). Figure 4 shows the same graph for all stages of the refracturing well (well 2). As the plots show, during fracturing, the microseismic response is almost instantaneous with the onset of pumping; whereas, in the case of refracturing, it takes several hours of pumping and several thousand barrels of slurry before any microseismicity is observed.

Figure 2 and Figure 4 show a progressive increase in event count per pumping stage during the refracturing treatments. The last five pumping stages in Figure 4 show considerably more events than the middle stages. The difference in the microseismic response to fracturing and to refracturing indicates the different stimulation mechanisms that are mobilized during each treatment. This will be discussed further in Section 4: Geomechanics of Refracturing.

3. Localized Stimulation at the Heel

The two potential contributing factors to the observed concentration of microseismicity at the heel are:

i. Pressure drop due to friction along the well
ii. Failure of diverters to seal off the perforations and move the fluid along the lateral after each pumping cycle

In order to investigate the effect of these two factors, we numerically simulated a generic refracturing treatment using a 3D finite difference code. We studied two extreme cases, fully effective diverters and non-effective diverters. The microseismic response to treatment was captured by implementing an implicit discrete fracture network (DFN) and monitoring the shear failure on each fracture throughout the simulation. The pressure drop along the well was calculated on a real-time basis, and the well pressure profile was continuously updated.

In the model representing the fully effective diverters, the diverters were modeled by closing the entry points (perforations) after each pumping stage. Two entry points were shut down after each stage, starting from the ones closer to the heel and moving down toward the toe. In the second model, which represents non-effective diverters, all perforations remained open throughout the simulation. A twelve-stage refracturing was simulated by this model. Each pumping stage consisted of 90 minutes of pumping at 60 bbl/min followed by a 20-minute pump break.

3.1. Numerical Model Setup

The numerical model represents a 6,400-ft lateral with 61 perforations, including 31 old perforations and 30 new perforations. Each new perforation was added between two consecutive old perforations, reducing the initial perforation spacing from 206 ft to 103 ft.

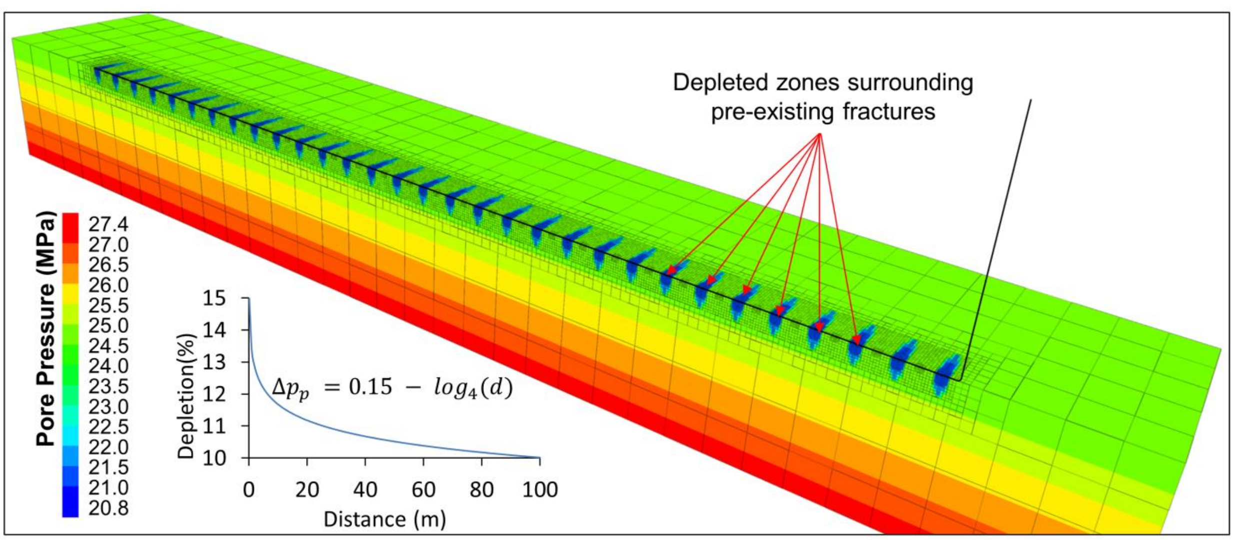

Figure 5: Pore pressure contours and depleted zones around pre-existing hydraulic fractures. Reservoir pressure depletion follows a logarithmic function of distance with a maximum depletion ratio of 15% at the lateral. The lateral extends 6,400 ft and includes 31 old perforations (206 ft apart) and 30 new perforations, added between the old ones, reducing the perforation distance to 103 ft for refracturing.

A normal faulting stress regime (S_v>S_{Hmax}> S_{hmin}) was applied in the model, with the minimum horizontal stress (S_{hmin}) direction parallel to the lateral. Gravitational stresses were initialized assuming a rock density of 2,600 kg/m^3. An isotropic horizontal stress state was considered with the magnitude of horizontal stresses being S_{Hmax}= S_{hmin}=0.8S_v. A hydrostatic pore pressure distribution was considered in the model.

The effect of previous production on reservoir pressure and stresses was taken into account by applying a depletion pattern around the pre-existing bi-wing planar fractures implemented in the model. The maximum pressure depletion was assumed to be 15% (of the initial pressure) at the well location, which dropped quickly with distance from the well, following a logarithmic relationship, as depicted in Figure 5. The current state of stresses were obtained by running the model to equilibrium after applying the depleted pressures. The background DFN consisted of two sub-vertical fracture sets, perpendicular to each other (Figure 6).

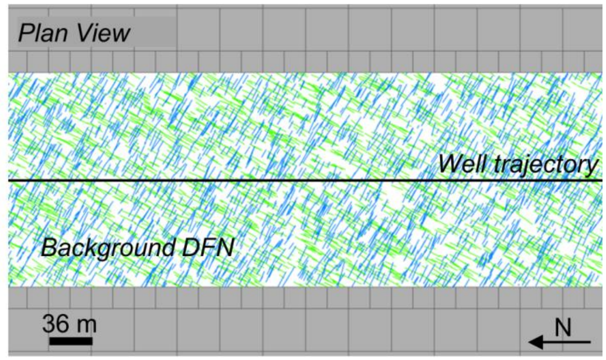

Figure 6: Horizontal section at the well depth showing the background DFN in the numerical models. Set 1 (blue): 90°/30°±5 (dip/dip direction) and Set 2 (green): 90°/120°±5 (dip/dip direction).

3.2. Pressure Losses along Lateral

The pressure drop at each segment along the well can be calculated using the Darcy-Weisbach Equation, as follows (Munson et al. 2012):

$$\Delta p = f \times \frac{L}{D} \times \frac{\rho}{2} \times v^2 \qquad (1)$$

where:

Δp: pressure drop

f: pipe friction coefficient

L: well length

D: well diameter

ρ: fluid density

v: flow velocity

The pipe friction coefficient, f, is calculated from the following equations for laminar and turbulent flow, respectively:

$$f = \frac{64}{R_e} \qquad (2) \qquad \text{(For laminar flow)}$$

$$\frac{1}{\sqrt{f}} = -2log_{10}\left(\frac{e}{3.7\,D} + \frac{2.51}{R_e\sqrt{f}}\right) \qquad (3) \qquad \text{(For turbulent flow)}$$

where R_e is the Reynolds number, and e is the roughness height of the casing in the unit of length. Equation 3 is known as the Colebrook-White Equation and applies when $R_e > 4{,}000$. Considering the common casing sizes (4½ inch) and injection rates for refracturing (>50 bbl/min), the flow is always turbulent, suggesting Equation 3 applies in most cases. The casing friction coefficient can also be estimated from the Moody chart (Munson et al. 2012). The Reynolds number is calculated from the following equation:

$$R_e = \frac{\rho v D}{\mu} \qquad (4)$$

where ρ is fluid density, and μ is fluid dynamic viscosity. For a common casing diameter of 4½ inches, the pressure drop rate along the lateral can reach as high as 0.6–0.9 psi/ft, depending upon the casing roughness ($e = 0 - 0.1$ mm), at the flow rate of q = 60 bbl/min for a slick water treatment ($\mu = 2.5$ cP). This suggests that for the common lateral lengths of 5,000–7,500 ft, the pressure contrast between the heel and the toe can theoretically reach as high as a few thousand psi. However, in a refracturing well, the pressure drop rate is not constant along the well but varies as a function of flow rate at each length interval of the well separated by two consecutive perforations (Figure 7).

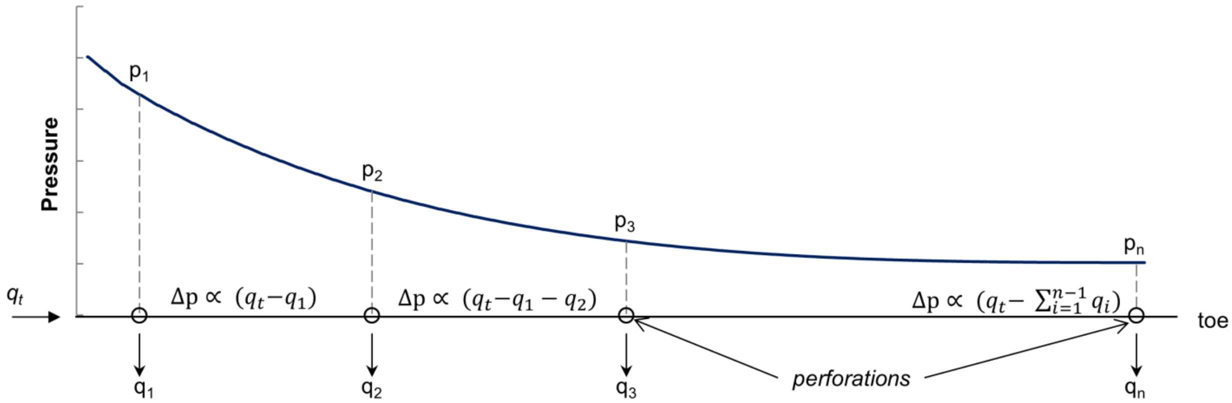

Figure 7: Schematic pressure profile along a horizontal well during refracturing. The pressure drop rate is not constant along the lateral due to discharge from perforations (q_i). The actual flow rate between two consecutive perforations is calculated by considering the discharge from perforations.

The pressure drop formulation was implemented in the simulations to calculate the correct pressure profile along the well at each time step of simulation. Figure 8 shows the evolution of the well pressure profile during the first 60 minutes of the first pumping stage, obtained from the numerical simulation. As the flow rate rises, the pressure profile diverges from the initial flat line and gradually becomes steeper until the target flow rate of 60 bbl/min is reached. After this point, the slope of the pressure profile remains almost constant during the rest of the stage. In this case, an injection pressure contrast of about 1,600 psi forms between the heel and the toe.

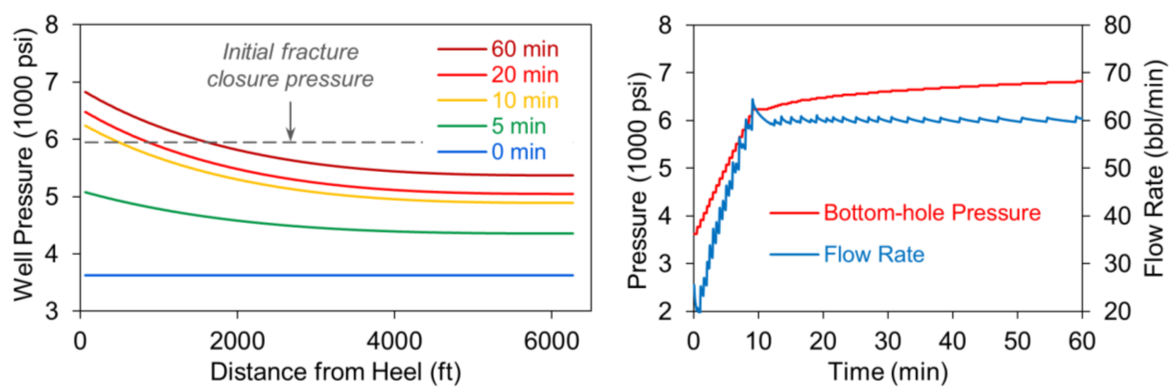

Figure 8: Evolution of pressure profile during the first 60 minutes of the first stage of the simulations. Pressure profile gradually becomes steeper as the flow rate increases, until the target flow rate is reached. A pressure contrast of about 1,600 psi is developed under the constant flow rate of 60 bbl/min.

3.3. Diverter Efficiency

Figure 9 shows the flow rate and bottomhole pressure plot for both the fully effective diverter and non-effective diverter models. The increasing trend of treatment pressure in Figure 9 is consistent with the field observations in most refracturing cases; the treatment pressure rises after each pumping cycle during the treatment. This trend is usually interpreted as an indication of diverter efficiency. However, as Figure 9 shows, the pressure can rise (though probably to a lesser extent) even when no diverters are applied. In this case, the increase of treatment pressure would be related to the gradual increase of reservoir pressure during the treatment, which results in the progressive reduction of pressure gradient between the well and the reservoir. Under this condition, the injection pressure must be constantly increased in order to reach and maintain the design flow rate. The amount of pressure increase depends on several factors, including previous stage pumping time, pump break time, reservoir permeability, reservoir isolation, fluid viscosity, and other factors. For the simulated cases, the pressure increase for the case with no diverter was about 700 psi after 12 pumping stages; while for the case with diverter, it was 2,700 psi.

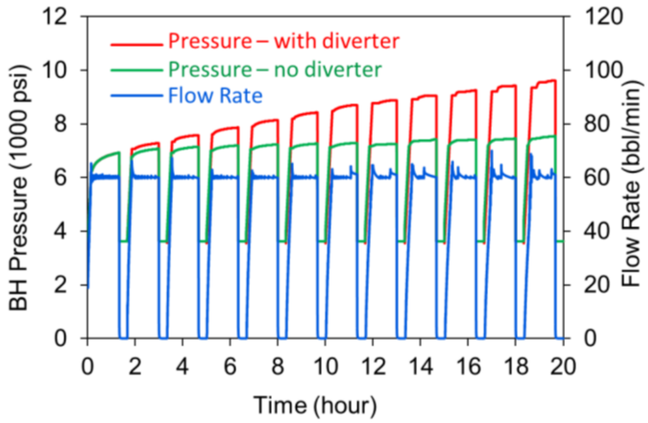

Figure 9: Flow rate and bottomhole pressure plots for 12-stage refracturing simulations.

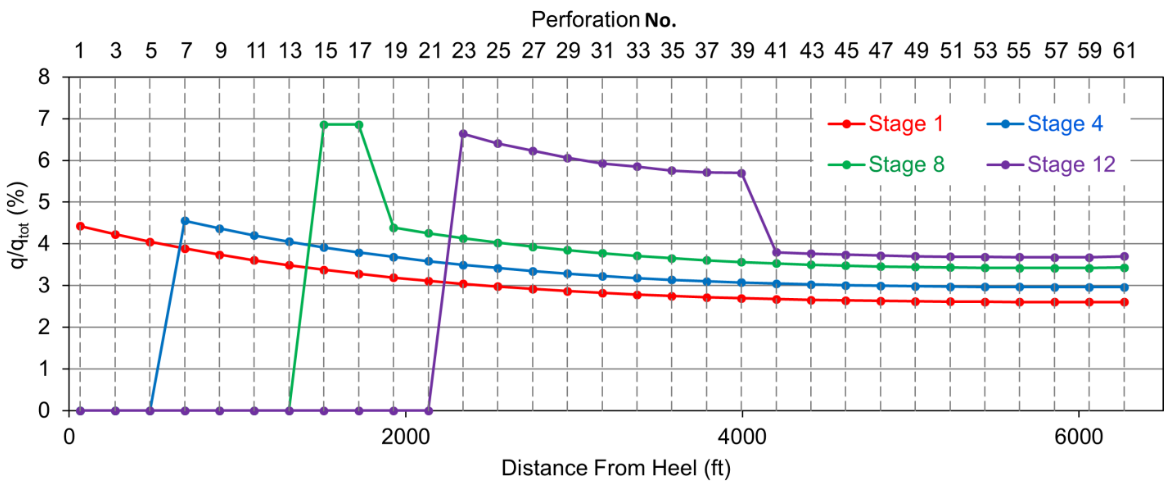

Figure 10: Perforation discharge profile (old perforations) for the with-diverter model at four stages of the treatment.

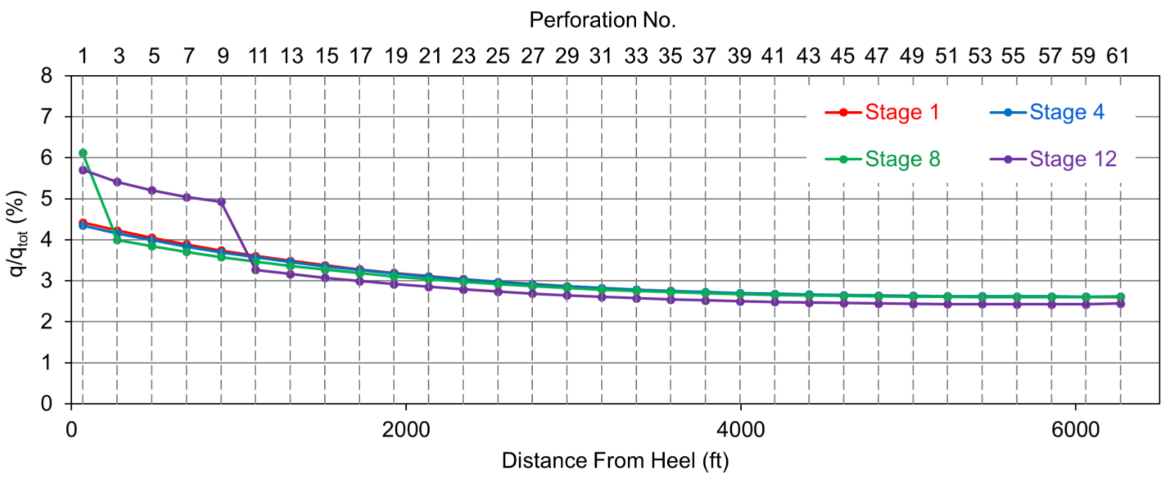

Figure 11: Perforation discharge profile (old perforations) for the no-diverter model at four stages of the treatment.

The perforation discharge profiles along the lateral are shown in Figure 10 and 11 for four pumping stages. In both cases, the discharge rate is initially higher at the heel and diminishes toward the toe, which is consistent with the well pressure profile shown in Figure 8. In the first model (fully effective diverter) the discharge profile changes as perforations are plugged off after each pumping stage; therefore, the high discharge front shifts gradually from the heel toward the toe as treatment continues (Figure 10Figure 10).

In the second model (non-effective diverter), however, the discharge profile remains almost unchanged during all stages of the simulation. In both cases, the sudden spike in discharge rate at any given perforation is associated with the re-opening of the pre-existing hydraulic fractures, which rapidly increases the conductivity of that fracture and the discharge rate of the corresponding perforation (fracture conductivity is proportional to the cube of fracture aperture). This occurs when the well pressure at any given perforation exceeds the formation fracture closure pressure, and a positive net pressure develops inside the fracture.

The synthetic microseismic events for both simulated cases are shown in Figure 12Figure 12 and Figure 13. The synthetic microseismic event distribution for the non-effective diverter model matches closely with the field microseismic events shown in Figure 1Figure 1, suggesting that the same factors contributed to the localized stimulation at the heel in those real cases.

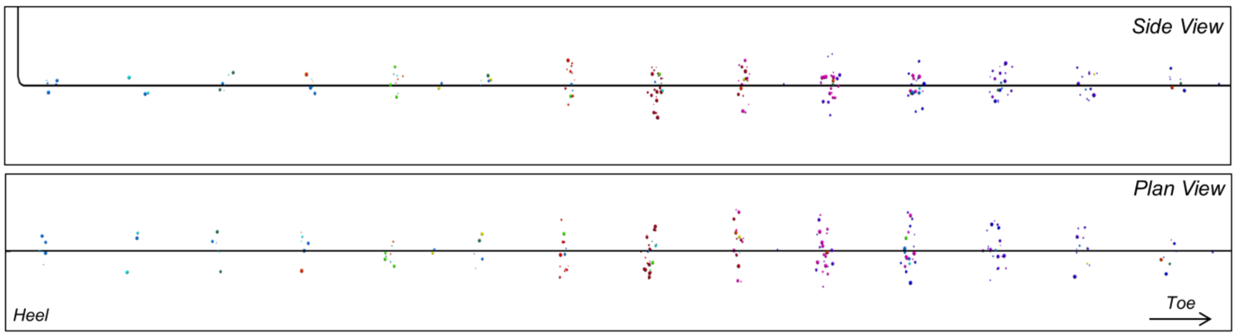

Figure 12: Synthetic microseismic events for the fully-effective-diverter model. Only the first half length of the lateral (28 perforations) is shown.

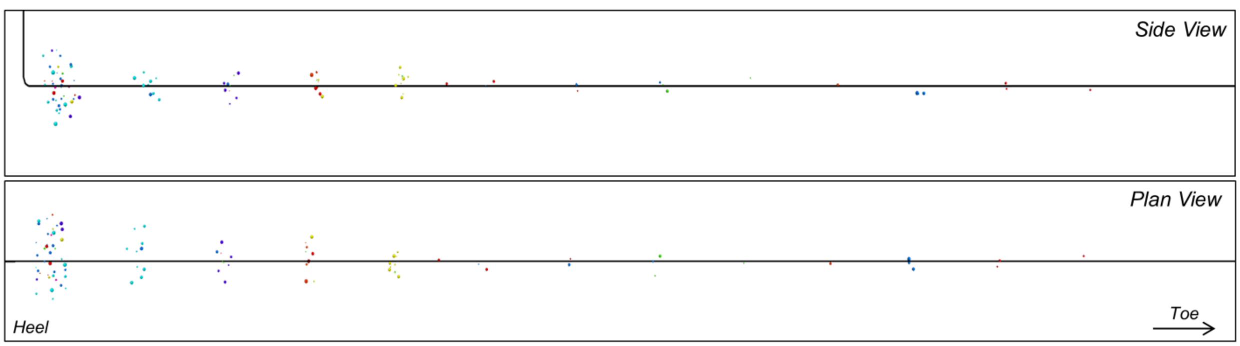

Figure 13: Synthetic microseismic events for the non-effective-diverter model. Only the first half length of the lateral (28 perforations) is shown.

4. Geomechanics of Refracturing

There are three important factors that differentiate refracturing from fracturing, from a geomechanical perspective:

1. Altered reservoir stresses due to production
2. Existence of the previously stimulated propped or un-propped fractures, which provide pathways to the injected fluid, even without breaking new rock
3. Increased flow capacity of the formation due to previous stimulations

4.1. Production-Induced Stress Changes

Before discussing the effect of production on reservoir stresses, it is important to clarify the terminology that we use in this regard. In a porous material where the void spaces are filled with fluid or gas, such as the reservoir rock, two types of stresses can be defined: total stress and effective stress. The total stress (σ) is the stress imposed by any external force, such as the weight of overburden rock or tectonic forces. The effective stress (σ'), on the other hand, is the actual stress felt by rock grains or matrix. These two stresses are related two each other by the following equation:

$$\sigma' = \sigma - \alpha p \qquad (5)$$

where α is the Biot's coefficient, and p is the pressure of fluid (or gas) trapped in the pore spaces. Equation 5 indicates that a part of the applied external load is taken by the fluid in the pore spaces, and only a portion of that load is transferred to the rock matrix. The importance of this separation is that it is the effective stress that controls rock deformation and failure (simply because this is the stress that is felt by rock matrix).

Production affects both total and effective stresses, but in two different ways; it increases the effective stresses but potentially reduces the total stresses. The depletion of reservoir pressure results in the increase of effective stresses, and consequently the deformation of the rock matrix under higher effective stresses, until a new equilibrium state is reached. In reservoirs with a relatively large drainage area (laterally), this phenomenon results in the subsidence of the overburden rock. Since the weight of overburden rock is fixed, the total stress remains almost unchanged.

But in the case of most unconventional reservoirs, where the drainage area is small in the vertical and one of the horizontal directions (usually S_{Hmax} direction) but relatively large in the other horizontal direction (along the horizontal well or usually S_{hmin} direction), the changes in total stresses are more complex. In these cases, most of the rock deformation occurs in the direction of maximum drainage length (or along the well). Since the surrounding rock is not free to move horizontally (as it is in the vertical direction) this results in the relaxation of total stresses along the well. The extent to which the total stresses decrease depends on the pressure depletion ratio and the poro-elastic properties of the rock, i.e., Biot's coefficient and modulus.

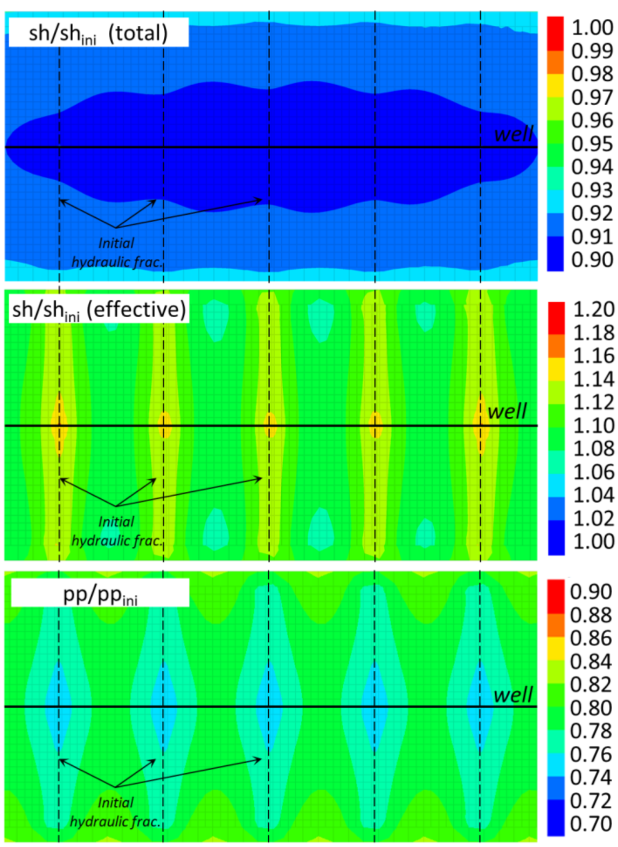

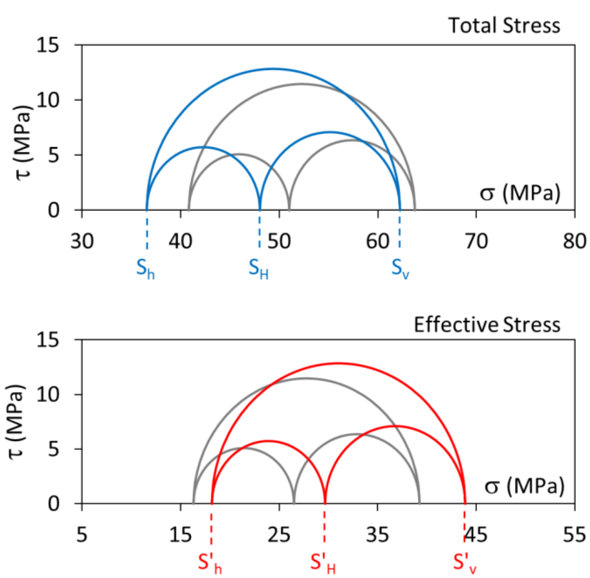

Figure 14: Numerical simulation of production in an initially stimulated reservoir. Contours show the ratio of current state (after 1 month of production) to initial state (before production) for total minimum stress (top), effective minimum stress (middle), and pore pressure (bottom). The Mohr circles (right) represent the full state of total and effective stresses before and after production.

The impact of production on effective and total stresses was numerically simulated using the same model that was built for refracturing. A semi-coupled fluid-mechanical simulation was run to simulate one month of production. Figure 14 shows the minimum horizontal stress and pore pressure contours along the well after one month of production. The contours show the ratio of the current state to the initial state for the minimum effective stress (S'_{hmin}), minimum total stress (S_{hmin}), and pore pressure. The Mohr circles represent the full state of stress (effective and total) at the center of the well length. In this simulation, a Biot's coefficient of α = 0.9 was considered. After one month of production, the Mohr circles representing the total stresses shifted to the left (lower stress), while the circles representing the effective stresses shifted to the right (higher stress). The change of the Mohr circle diameters during production indicates that not only does the absolute magnitude of stresses change during production, but so does the relative magnitude.

Consistent with the above explanation, the maximum total stress reduction occurred in the S_{hmin} direction (parallel to the well), and the minimum total stress change occurred in the vertical direction. In the case of effective stresses, this order is reversed; the maximum change in effective stress occurred in the vertical direction, while the minimum change in effective stress occurred in the S_{hmin} direction. This is basically due to the fact that pore pressure changes isotropically, but total stresses change anisotropically during production. An important point that can be made here is that production potentially increases stress anisotropy. Considering that stress anisotropy is the main driving force for stimulation of natural fractures, it can be argued that production acts in favor of re-stimulation, because it puts natural fractures in a more critically stressed state.

4.2. Fracture Initiation versus Fracture Re-Opening

In a refracturing treatment, new perforations are commonly added between the old ones in an effort to create new transverse fractures and contact fresh rock. For a new fracture to initiate and propagate from these new perforations, three conditions must be met:

- Well pressure must exceed the available rock strength and stresses to initiate a new fracture (fracture initiation pressure or formation breakdown pressure).
- The fluid pressure inside the fracture must exceed the formation minimum pressure (likely S_{hmin}) to develop a positive net pressure (P_{net}=fracture fluid pressure – minimum formation pressure) , which keeps the fracture open.
- The treatment flow rate must exceed the flow capacity of the rock (or leakoff rate from the open fracture) in order to maintain the net pressure and force the fracture to propagate away from the wellbore

Old perforations, on the other hand, are already in hydraulic connection with the pre-existing fractures, which can take fluid without breaking new rock. The difference between these two types of perforations can be better understood by referring to the schematic mini-frac test plot shown in Figure 15. As the plot shows, in the case of new perforations, the well pressure must first reach the formation breakdown pressure (FBP) to break the intact rock and initiate a new hydraulic fracture. After this point, the pressure must be maintained at the fracture propagation pressure (FPP) in order to extend the created fracture. In the case of old perforations, once the treatment pressure exceeds the fracture closure pressure (FCP), the pre-existing fractures will dilate and start taking more fluid. Considering the FCP is less than both FBP and FPP, the re-opening of the pre-existing fractures will occur first, before the new rock can be broken at the new perforations.

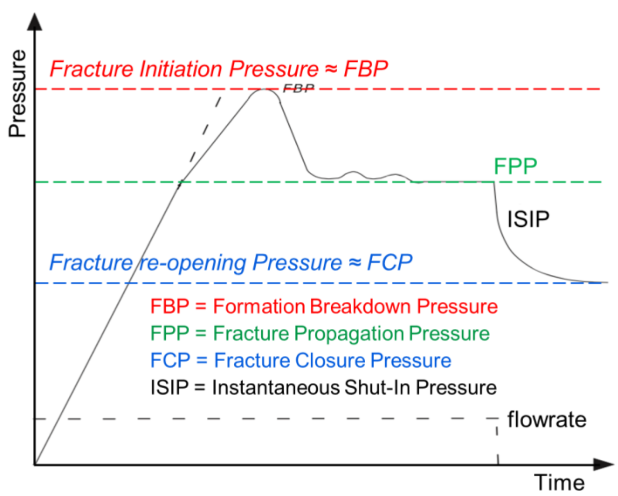

Figure 15: Schematic mini-frac pressure-time graph

An important point that must be noted here is that the failure of fresh rock, or fracture initiation, is controlled by the effective stresses, whereas the re-opening of pre-existing fractures is controlled by the total stresses; that is, they open once the fluid pressure developed inside the fractures exceeds the total stresses acting on their plane (usually S_{hmin}). Considering the effects of production on effective and total stresses (Figure 14), we can conclude that production potentially acts in favor of re-opening of the pre-existing fractures by lowering FCP and against creating new fractures by increasing FBP.

The above arguments are consistent with the lower apparent ISIPs typically observed during early stages of refracturing compared to the original ISIPs for the same well (or pad) (Figure 16). This suggests that the recorded ISIPs during refracturing are more related to re-opening of the pre-existing fractures than creation of new hydraulic fractures. As treatment continues, the buildup of pore pressure around the pre-existing fractures results in the increase of total stresses in the reservoir (reverses the production effect), which is reflected as progressively increasing apparent ISIP or treating pressure during refracturing (Figure 16).

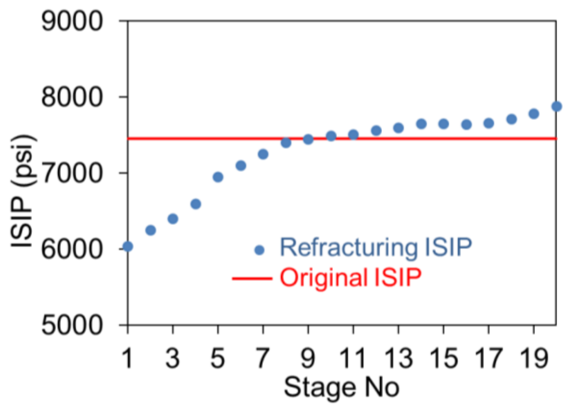

Figure 16: Apparent ISIPs (blue dots) for 20 stages of a refracturing treatment (well C in Figure 1). The red solid line shows the fresh rock ISIP recorded during the fracturing of the same well.

4.3. Fracture Propagation in a Formation with Increased Flow Capacity

An important factor in the design of hydraulic fracturing treatments is the applied injection rate relative to the flow capacity of the formation (or leakoff rate). After a fracture is initiated, it will propagate if the injection rate into the fracture exceeds the flow capacity of the formation (Nagel 2015). In other words, a fracture will propagate if the total volume of injected fluid per unit of time is greater than the leakoff rate into the formation, causing a fracture volume to be created inside the rock. If, at any point during pumping, this balance becomes negative, the fracture propagation will stop, and the fracture will close down.

In most refracturing cases, the applied injection rate is almost similar to the rate that was used for initial fracturing of one stage of the well. In the Haynesville and Eagle Ford wells, this rate is typically 60–70 bbl/min. Considering that during refracturing, all perforations (old and new ones) are open to take fluid simultaneously, the effective flow rate at each perforation will be way below the flow capacity of the formation. This implies that even if we manage to initiate new fractures from the new perforations, there will not be enough flow rate (hydraulic energy) available to extend those fresh fractures between the two pre-existing fractures with high hydraulic conductivity.

The above arguments suggest that, if no mechanical stage isolation is applied and the diverters fail to completely plug off old perforations, it is very unlikely to create new transverse hydraulic fractures from new perforations added between two old ones. This is more important in the more recent wells where initial stage spacing is smaller (usually <300 ft), as opposed to older wells that were initially stimulated using a larger stage spacing.

4.4. Dominant Stimulation Mechanism

If creating new hydraulic fractures is unlikely by refracturing, what is the main stimulation mechanism? The short answer is “stimulation of natural fractures,” but how? We can answer this question by referring to the observed microseismic responses shown in Figure 1 and 2 and the geomechanical principles governing rock failure and microseismicity.

Microseismicity is the acoustic representation of rock failure. When rock breaks, either in shear or in tension, the elastic strain energy stored in the rock is released and generates an elastic wave that is captured by the geophones and recorded as a microseismic event. Since the level of energy released upon opening of rock fractures is usually low during fracturing/refracturing (less than the sensitivity of the geophones), most of the microseismic events are associated with shear failures. The shear failure of rocks usually follows the Mohr-Coulomb failure criterion:

$$\tau = c + (\tan\varphi)\,\sigma_n' \qquad (6)$$

where τ is shear stress, c is cohesion, φ is the internal friction angle, and σ_n' is the effective normal stress acting on the fracture plane, which is equal to $\sigma_n' = \sigma_n - p$, where σ_n is the total normal stress, and p is the fluid pressure.

Based on this failure criterion, a shear failure occurs if any of the following conditions is met:

1. The stresses acting on a weakness plane change so the resulting shear stress exceeds the available shear strength (commonly referred to as "dry" microseismic events).
2. Pore pressure rises so that the available shear strength drops below the shear stress acting on the weakness plane (commonly referred to as "wet" microseismic events).

The shear stimulation due to changes in stresses is mainly driven by the propagation of a new hydraulic fracture. Agharazi et al. (2013) and Nagel et al. (2014) showed that a high shear zone develops at the tip of a propagating hydraulic fracture that moves with the propagating fracture tip. Natural fractures that fall inside this shear zone experience an increase in shear stresses and may slip, depending upon their orientation and shear strength characteristics. These failures are dry events since they are purely driven by stress changes (no fluid pressure change involved). Because these events are associated with the propagation of the hydraulic fractures, they are expected to be observed during the early seconds or minutes of pumping.

Behind the shear zone, a compressive zone forms on either side of the fracture with lower shear stresses (Agharazi et al. 2013 and Nagel et al. 2014). Within this region, the buildup of pore pressure due to fluid leakoff into formation is the only mechanism that can cause shear failure (wet events) on natural fractures.

During refracturing, however, no major fresh hydraulic fracture develops, as discussed in the previous section. Therefore, no major change of shear stress on natural fractures is expected. In this case, the dominant stimulation mechanism will be the pore pressure-driven shear slippage of natural fractures, which takes place by the increase of reservoir pressure during refracturing. For this mechanism to be effective, the pore pressure must be raised to a critical level at which the available shear strength on weakness planes fall below the active shear stress. This mechanism is graphically represented by shifting the Mohr circles toward the Mohr-Coulomb failure envelope (less effective stress), as shown in Figure 17.

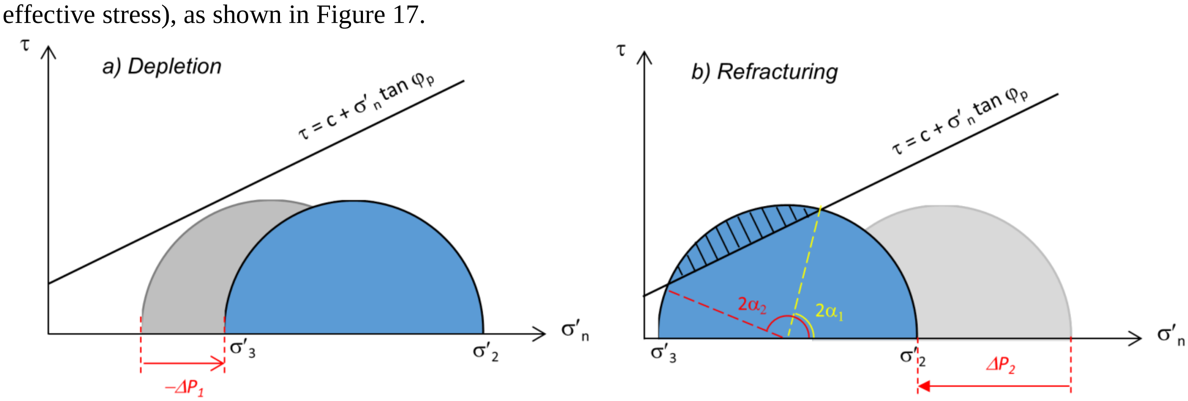

Figure 17: Mohr circles schematically showing the variation of effective stresses on weakness planes during a) depletion and b) refracturing. By injecting the fluid during refracturing, the pore pressure on weakness planes increases by ΔP_2 resulting in failure of weakness planes oriented at angles between α_1 and α_2 (measured as the angle between normal to the plan and σ_2 direction).

Due to the low permeability of unconventional reservoirs and the prior pressure depletion caused by production, the increase of pressure to the critical level is a lengthy process and usually takes several hours of pumping and several thousand barrels of slurry. This explains the frequently observed long delay in microseismic response to refracturing, as shown in Figure 2, and the high volume of slurry injected into the lateral during this time (Figure 2 and Figure 4) This mechanism is also consistent with the observed increase of event count per pumping stage, as shown in Figure 4.

In a low permeability rock such as unconventional reservoirs, pore pressure can be increased in two ways; first, directly, by injecting high pressure fluid into the rock, and second, indirectly, by rapid loading of the rock (undrained loading). In the second case, the pore pressure builds up due to rock deformation (poro-elastic effect) (Jaeger et al. 2007, Detournay and Cheng 1993). When the rate of loading (increase of net pressure on the fracture surface) is higher than the pressure diffusion rate, the excess pore pressure generated by rock deformation cannot dissipate at the same pace as the rock (pores) deforms, resulting in the buildup of pore pressure. The level of pore pressure increase under such loading conditions depends upon several factors, including Biot's modulus, Biot's coefficient, and the rate of loading. Given the nano-Darcy permeability of unconventional reservoirs, the common rate of loading in most fracturing treatments is high enough to generate some pore pressure in an indirect fashion.

This effect was numerically simulated for a single fracture with a height of 262 ft and maximum length of 787 ft. The maximum net pressure (fluid pressure minus S_{hmin}) of 300 psi, acting at the fracture center, was applied over a course of 2 minutes. The maximum induced fracture width was measured as w_{max}= 13.8 mm at the fracture center. Figure 18 shows the pore pressure increase contours (ratio of current pore pressure to initial pore pressure) on a horizontal section crossing the center of the fracture. The illustrated pore pressure buildup is solely due to the inflation of the fracture under the applied load and does not include any leakoff effect.

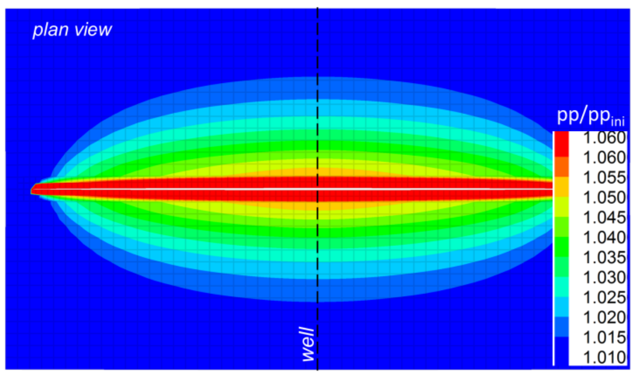

Figure 18: Excess pore pressure generated solely by the deformation of rock under a positive net pressure inside the hydraulic fracture (no leakoff involved). The contours represent the ratio of current pressure to the initial value for a fracture with maximum total length of 787 ft. The maximum net pressure and width at the fracture center are 300 psi and 13.8 mm, respectively. (Mesh deformation exaggerated by a factor of 50.)

5. An Optimized Refracturing Design

We developed and numerically examined an alternative refracturing method based on the microseismic observations and geomechanical studies described in the previous sections. The fundamental assumption of this method is that the dominant stimulation mechanism is the pore pressure-driven shear stimulation of natural fractures. Therefore, the treatment design mainly aims to increase the productive complexity within the reservoir. It also improves fluid conductivity of the pre-existing fractures.

The proposed method consists of two steps per pumping cycle, a slow pressurization step, during which fluid pressure gradually builds up inside natural and induced fractures, followed by a stimulation step, during which high injection pressures are applied to initiate shear failures on critically stressed natural fractures (Figure 19).

During the first step, the fracturing fluid is injected into the well at a constant pressure, set just below the FCP of the formation. It is important to keep the injection pressure below FCP at this stage to avoid excessive dilation of the pre-existing fractures closer to the heel. The sole purpose of this step is to increase pressure in the reservoir in order to put more natural fractures at the critical stress state. Because no stimulation is intended during this stage, no proppant should be added to the fluid. Any proppant injected at this stage will increase the resistance to the flow and will minimize the extent of the pressurized zone. The first step is considered complete when the rate of flow-rate drop under constant injection pressure becomes slow. Depending upon the reservoir permeability and pressure state, this stage can take up to a few hours. Longer pumping time and lower viscosity help to increase the extent of the pressurized zone at this stage. Note that pressure diffusion is inversely related to fluid viscosity (Jaeger et al. 2007).

Once the pressurization stage is complete, to switch to the next step, the injection pressure is increased until the target flow rate is reached. Very high flow rates should be avoided at this stage to keep the pressure drop rate low and to maintain a relatively uniform pressure profile along the lateral. Note that the pressure drop is proportional to the square of flow rate, so any small increase in flow rate will result in a considerable increase in the pressure drop rate (Equation 1). Proppant should be added to the slurry at this stage. Fluids with higher viscosities can be used to lower the flow rate while maintaining the high injection pressure during this stage. The minimum flow rate, however, should be selected by considering the proppant transport capability of the slurry in order to avoid early screenouts. Higher viscosity also shifts the pore pressure generation mechanism from flow-dependent (pressure diffusion) in step 1 to rock deformation-dependent (poro-elastic effect) in step 2.

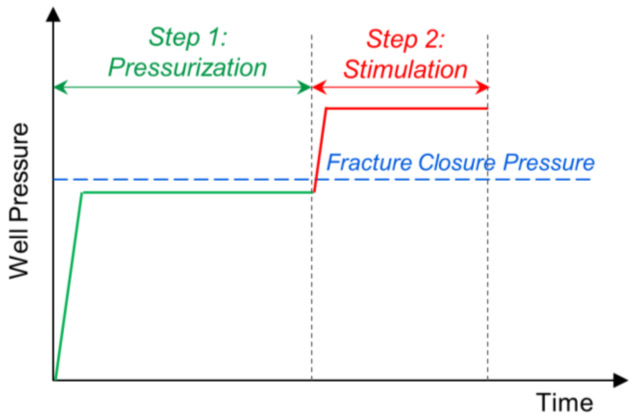

Figure 19: Schematic graph showing the treatment steps per pumping stage for the two-step refracturing method.

Several pumping cycles should be performed to enhance the stimulation efficiency. The pump break time between the treatment cycles must be kept short to minimize the dissipation of the excess pressure generated during the previous pumping stages. Considering the increase of formation closure pressure with pore pressure, the injection pressure of step 1 must also be increased after each pumping stage.

5.2. Numerical Simulation

We numerically simulated one pumping stage of the proposed method. Two cases were studied. In the first case, slickwater (SW) (μ = 2.5 cP) was injected during both steps. In the second case, slickwater (μ = 2.5 cP) was injected during the first step, and linear gel (LG) (μ = 20 cP) during the second step. Pump curves for both cases are shown in Figure 20.

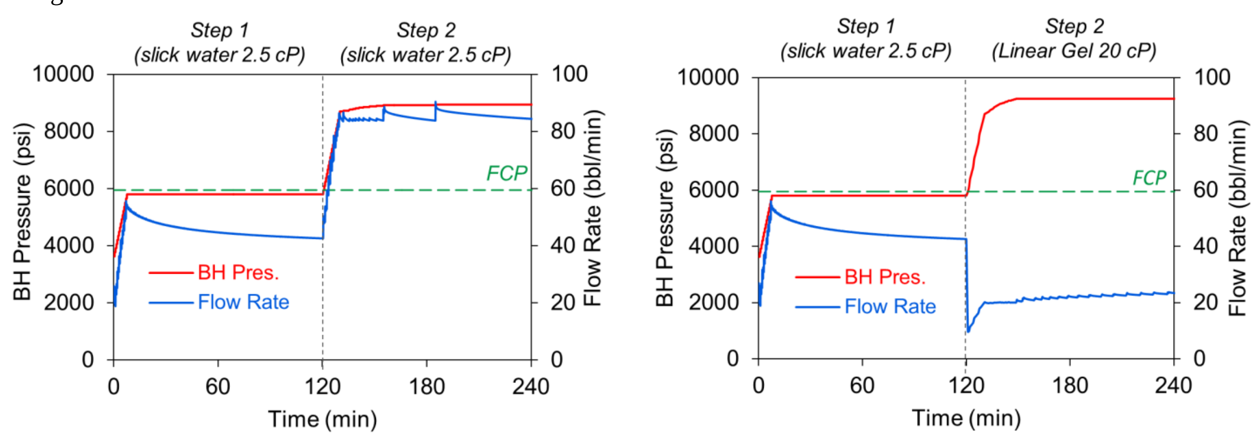

Figure 20: Bottomhole pressure and flow rate graphs for the two-step refracturing numerical model. In both simulations, slickwater with viscosity of μ = 2.5 cP was used for the pressurization step. Two fluids were used for the second step: slickwater (left graph) and linear gel (μ = 20 cP) (right graph).

During the pressurization stage (step 1) the injection pressure was kept at P_w=5800 psi (40 MPa), just below the formation closure pressure *FCP*=5950 psi (41 MPa). The first step was complete after 2 hours, when the flow rate dropped to almost a constant value of q=43 bbl/min (Figure 20). The injection pressure was then increased to the design bottomhole pressure of P_w = 9200 psi to switch to the second step.

Figure 21 shows the pressure and discharge rate profiles for both models. In the SW-SW case a high pressure contrast developed along the lateral that led to a non-uniform discharge profile with high discharge rates at the heel. Increasing fluid viscosity at step 2 in the SW-LG model dropped the flow rate sharply, leading to uniform pressure and discharge profiles along the lateral. Note that no friction reducer was considered in these simulations. Adding friction reducer will lower the pressure contrast during the second step of the SW-SW model.

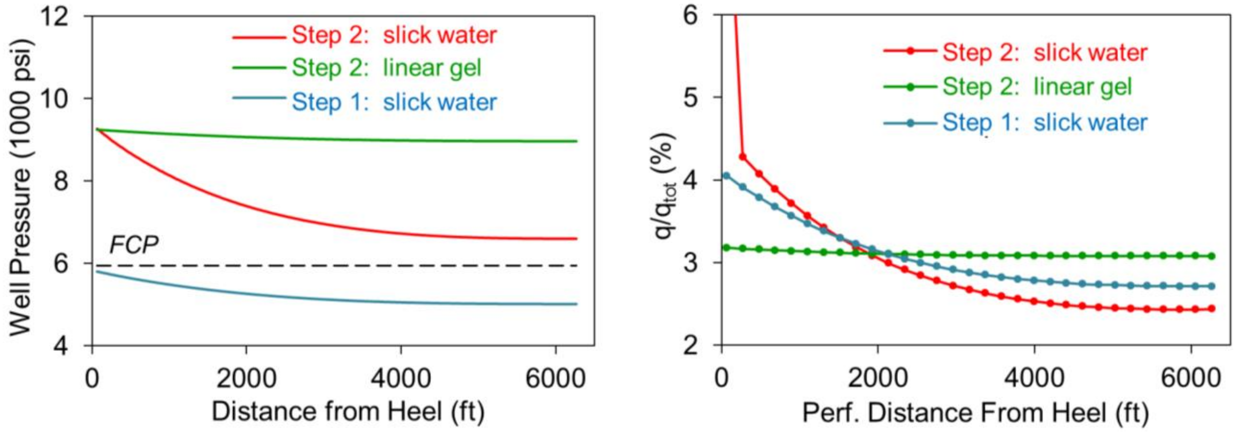

Figure 21: Well pressure (left) and discharge ratio (right) profiles for the simulated two-step cases: SW-SW and SW-LG.

The evolution of pore pressure on natural fractures during both stages of the treatment is shown in Figure 22 for the SW-LG case. The synthetic microseismic events associated with the SW-LG model are also shown in Figure 23. As shown in Figure 23, a uniform microseismic event distribution developed along the lateral, indicating a uniform stimulation of the reservoir by the treatment.

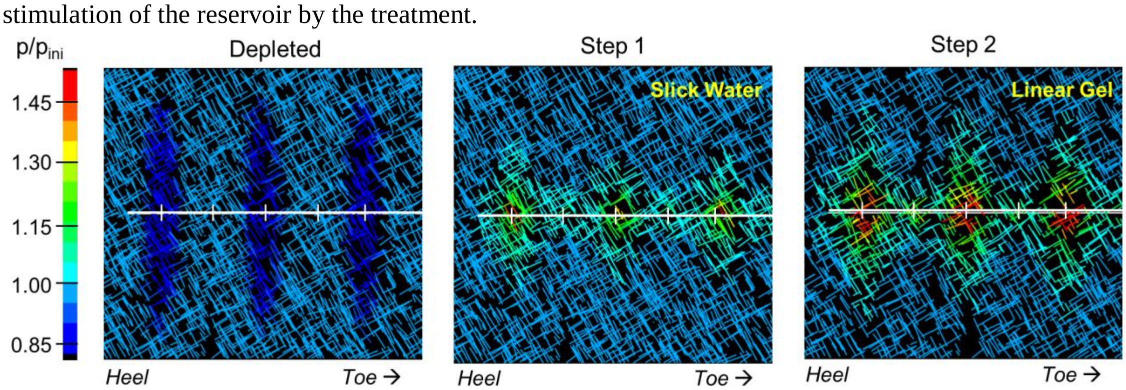

Figure 22: Evolution of pore pressure on natural fractures during the two-step SW-LG treatment simulation (just the first 600 ft of the well is shown).

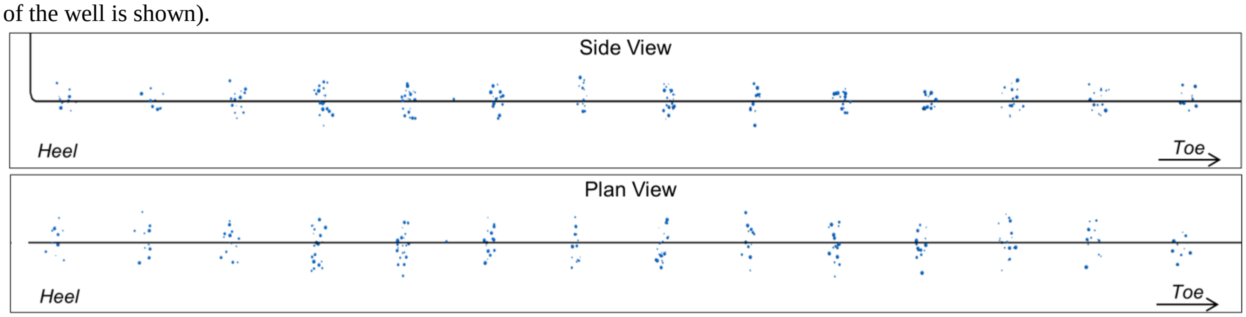

Figure 23: Synthetic microseismic events for the two-step SW-LG model (first half of the model is shown).

5.3. Best Candidates

Because the proposed method is based on shear stimulation of natural fractures by a pore pressure-driven mechanism, the following factors have a significant impact on the efficiency of the method and can be used as guidelines for selecting the best candidates for refracturing by this method:

- Stress anisotropy: Higher stress anisotropy increases active shear force on natural fractures, so less pore pressure is required to trigger failure.
- Fracture orientation relative to principal stresses direction: Assuming sub-vertical fractures, the most favorable orientation for shear failure is theoretically equal to $\beta=45-\varphi/2$ measured from s_{Hmax}, where □ is the friction angle of the fracture.
- Shear strength: Lower shear strength (lower c and φ needs less pressure for shear failure to occur.

Figure 24 shows the minimum pore pressure required to trigger shear failure on sub-vertical fractures of various orientations. The stresses and pore pressures correspond to the values used in the numerical simulations. The minimum required pore pressure is calculated for two stress anisotropies ($s_{Hmax}-s_{hmin}$) of 750 psi and 1500 psi. The graphs show how the required minimum pore pressure changes with the fracture orientation and stress anisotropy for a given fracture strength. It also shows that for reservoirs with originally higher pressure or those that are less depleted, it takes less pore pressure (energy) to trigger shear failure on natural fractures.

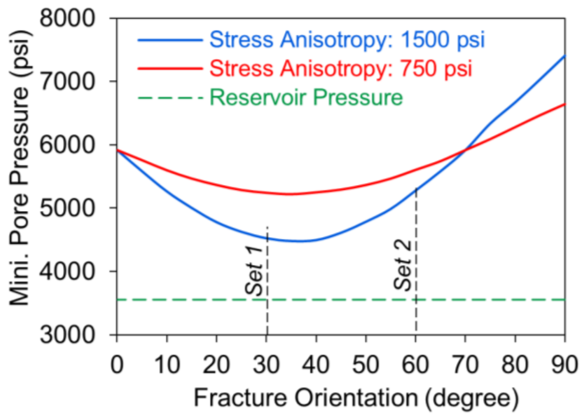

Figure 24: Variation of minimum pore pressure required to trigger shear failure on natural fractures for various sub-vertical fracture orientations. Two different horizontal stress anisotropies were considered. Dotted green line shows the reservoir pressure.

Considering the above factors, the proposed two-step refracturing treatment method is more efficient in the over-pressured reservoirs that are naturally fractured and have high stress anisotropy.

6. Conclusion

In this study, we numerically modeled refracturing in a 6,400-ft long horizontal well with 61 perforations. The study showed that the main factors causing the concentration of microseismic events at the heel were i) pressure drop along the lateral due to frictional forces and ii) inefficiency of the applied diverters.

Based on geomechanical principles, we demonstrated that if no mechanical isolation is used, it is unlikely that a fresh hydraulic fracture from new perforations will be able to propagate between two pre-existing fractures. In this situation, the dominant stimulation mechanism is the shear stimulation of natural fractures by a pore pressure-driven mechanism.

Given the nano-Darcy permeability of unconventional reservoirs, it takes several hours of pumping and several thousand barrels of slurry to build up enough pore pressure within the reservoir to trigger shear failure of natural fractures, which explains the frequently observed delay in microseismic response to refracturing.

Based on these conclusions, we proposed an alternative refracturing method that consists of two steps per pumping stage. The basic principles of this method are:

- Pressurizing the reservoir before stimulation under an injection pressure lower than the formation closure pressure.
- Stimulating the reservoir under high injection pressure while keeping the flow rate low to maintain uniform pressure and discharge profiles along the well.
- Repeating the same steps by running several pumping cycles and keeping the pump break time short.

The proposed refracturing method aims at increasing the reservoir productive complexity and enhancing the hydraulic conductivity of the pre-existing fractures. Because the main stimulation mechanism is shear failure of natural fractures, the best candidate wells for this method are those in naturally fractured reservoirs that have a high stress anisotropy and high pore pressure.

The key factors in the success of the proposed method are proper handling of injection pressures and flow rates with respect to the formation stresses and flow capacity in order to avoid localized stimulation of the well at the heel. Therefore, accurate estimation of the reservoir pressures and stresses along the well is critical to the treatment success. Geomechanical models and numerical simulations can be used to calculate the current state of stress before refracturing, based on the pressure depletion data and the original reservoir stresses. The initial completion information provides a valuable source of data for this purpose. Due to the stress/pressure changes induced by the treatment in the reservoir, the injection pressures must be updated after each pumping cycle.

Considering the uncertainties in the field data and stress and pressure heterogeneities along the well, real-time adjustments to the design parameters must be considered. Real-time microseismic monitoring provides a powerful means for onsite assessment of the treatment parameters and applying the necessary adjustments as treatment continues.

A proper combination of treatment fluid and pumping rate must be selected to maintain a relatively uniform pressure profile during both steps of the treatment while meeting the proppant transport requirements. The pressure drop must be calculated based on the well/casing specifications for each well

References

Agharazi, A., Lee, B., Nagel, N.B., Zhang, F., Sanchez, M. 2013. Tip-Effect Microseismicity – Numerically Evaluating the Geomechanical Causes for Focal Mechanisms and Microseismicity Magnitude at the Tip of a Propagating Hydraulic Fracture. SPE Paper 167129-MS Presented at the SPE Unconventional Resources Conference Canada, Calgary, Canada, 5–7 November.
Detournay, E., Cheng, A. 1993. Fundamentals of Poroelasticity. Online source: http://www.olemiss.edu/sciencenet/poronet/fundporo.pdf (accessed November 01, 2015).

Diakhate, M., Gazawi, A., Barree, B., Cossio, M., Tinnin, B., McDonald, B., Barzola, G. 2015. Refracturing on Horizontal Wells in the Eagle Ford Shale in South Texas – One Operator's Perspective. SPE Paper 173333-MS Presented at the SPE Hydraulic Fracturing Conference, The Woodlands, Texas, 3–5 February.

Jaeger, J.C., Cook, N.G.W., Zimmerman, R.W. 2007. Fundamentals of Rock Mechanics. 4th Edition. Blackwell Publishing Ltd.

Lantz, T.G., Greene, D.T., Eberhard, M.J., Norried, R.S., Pershall, R.A. 2007. Refracture Treatments Proving Successful In Horizontal Bakken Wells; Richland Co, MT. SPE Paper 108117-MS Presented at the Rocky Mountain Oil & Gas Technology Symposium, Denver, Colorado, 16–18 April.

Munson, B. R., Rothmayer, A.P., Okiishi, T.H., Huebsch, W.W. 2012. Fundamentals of Fluid Mechanics. 7th Edition. Wiley

Nagel, N. B., Sheibani, F., Lee, B., Agharazi, A., Zhang, F. 2014. Fully-Coupled Numerical Evaluations of Multiwell Completion Schemes: The Critical Role of In-Situ Pressure Changes and Well Configuration. SPE Paper 168581-MS Presented at the SPE Hydraulic Fracturing Technology Conference, The Woodlands, Texas, 4–6 February.

Nagel, N. B. 2015. Hydraulic Fracturing: Of Magic and Engineering. Online source: https://www.linkedin.com/pulse/hydraulic-fracturing-magic-engineering-continued-neal-nagel?trk=prof-post (accessed November 08, 2015).

Nomeli, M.A., 2014. Direct Numerical Simulation of Pore Scale Flow and Reactive Transport of CO^2 in Porous Media. American Geophysical Union, Fall Meeting, San Francisco, California , December 15–19. Abstract H11H-1012.

Sudhendu, K., Jbeili, T. 2015. Beating the decline through refracturing. *World Oil Journal*, June 2015.
Vincent, M. C. 2010. Refracs – Why Do They Work, And Why Do They Fail in 100 Published Field Studies? SPE Paper 134330-MS Presented at the SPE Annual Technical Conference and Exhibition, Florance, Italy, 19–22 September.

Zoback, M. D. 2010. Reservoir Geomechanics. *Cambridge University Press*